

See discussions, stats, and author profiles for this publication at: <https://www.researchgate.net/publication/41169544>

# Effects of Single Metal-Ion Doping on the Visible-Light Photoreactivity of TiO<sub>2</sub>

ARTICLE *in* THE JOURNAL OF PHYSICAL CHEMISTRY C · DECEMBER 2009

Impact Factor: 4.77 · DOI: 10.1021/jp908088x · Source: OAI

---

CITATIONS

290

READS

38

## 3 AUTHORS, INCLUDING:



Jina Choi

Korea Research Institute of Chemical Tech...

15 PUBLICATIONS 605 CITATIONS

[SEE PROFILE](#)



Michael R. Hoffmann

California Institute of Technology

417 PUBLICATIONS 30,420 CITATIONS

[SEE PROFILE](#)

## Effects of Single Metal-Ion Doping on the Visible-Light Photoreactivity of TiO<sub>2</sub>

Jina Choi,<sup>†</sup> Hyunwoong Park,<sup>‡</sup> and Michael R. Hoffmann\*,<sup>†</sup>

W. M. Keck Laboratories, California Institute of Technology, Pasadena, California 91125, and School of Physics and Energy Science, Kyungpook National University, Daegu 702-701, South Korea

Received: August 21, 2009; Revised Manuscript Received: November 10, 2009

Titanium dioxide (M-TiO<sub>2</sub>), which was doped with 13 different metal ions (i.e., silver (Ag<sup>+</sup>), rubidium (Rb<sup>+</sup>), nickel (Ni<sup>2+</sup>), cobalt (Co<sup>2+</sup>), copper (Cu<sup>2+</sup>), vanadium (V<sup>3+</sup>), ruthenium (Ru<sup>3+</sup>), iron (Fe<sup>3+</sup>), osmium (Os<sup>3+</sup>), yttrium (Y<sup>3+</sup>), lanthanum (La<sup>3+</sup>), platinum (Pt<sup>4+</sup>, Pt<sup>2+</sup>), and chromium (Cr<sup>3+</sup>, Cr<sup>6+</sup>)) at doping levels ranging from 0.1 to 1.0 at. %, was synthesized by standard sol–gel methods and characterized by X-ray diffraction, BET surface area measurement, SEM, and UV–vis diffuse reflectance spectroscopy. Doping with Pt(IV/II), Cr(III), V(III), and Fe(III) resulted in a lower anatase to rutile phase transformation (A–R phase transformation) temperature for the resultant TiO<sub>2</sub> particles, while doping with Ru(III) inhibited the A–R phase transformation. Metal-ion doping also resulted in a red shift of the photophysical response of TiO<sub>2</sub> that was reflected in an extended absorption in the visible region between 400 and 700 nm. In contrast, doping with Ag(I), Rb(I), Y(III), and La(III) did not result in a red shift of the absorption spectrum of TiO<sub>2</sub>. As confirmed by elemental composition analysis by energy dispersive X-ray spectroscopy, the latter group of ions was unable to be substituted for Ti(IV) in the crystalline matrix due to their incompatible ionic radii. The photocatalytic activities of doped TiO<sub>2</sub> samples were quantified in terms of the photobleaching of methylene blue, the oxidation of iodide (I<sup>−</sup>), and the oxidative degradation of phenol in aqueous solution both under visible-light irradiation ( $\lambda > 400$  nm) and under broader-band UV–vis irradiation ( $\lambda > 320$  nm). Pt- and Cr-doped TiO<sub>2</sub>, which had relatively high percentages of rutile in the particle phase, showed significantly enhanced visible-light photocatalytic activity for all three reaction classes.

### Introduction

Titania (TiO<sub>2</sub>) has been extensively studied as a photocatalyst for applications such as water and air remediation, because of its relatively high photocatalytic activity, robust chemical stability, relatively low production costs, and nontoxicity. Redox reactions of environmental interest are initiated on the TiO<sub>2</sub> surface with trapped electron–hole after band gap excitation. However, TiO<sub>2</sub> is active only under near-ultraviolet irradiation due to its wide band gap energy of 3.0–3.2 eV. Therefore, significant efforts have been made over the last 20 years to develop modified TiO<sub>2</sub> particles that are active under visible-light irradiation ( $\lambda > 400$  nm). Various strategies have been pursued including doping with metal ions (e.g., iron,<sup>1–3</sup> nickel,<sup>4,5</sup> vanadium,<sup>6–8</sup> and chromium<sup>9–11</sup>) or nonmetallic elements (e.g., nitrogen,<sup>12–14</sup> sulfur,<sup>15,16</sup> and carbon<sup>17,18</sup>).

Metal-ion-doped TiO<sub>2</sub> has been primarily studied to enhance the photocatalytic activity under UV irradiation.<sup>19–23</sup> Choi et al.<sup>19</sup> reported that doping with Fe<sup>3+</sup>, Ru<sup>3+</sup>, V<sup>4+</sup>, Mo<sup>5+</sup>, Os<sup>3+</sup>, Re<sup>5+</sup>, and Rh<sup>3+</sup> ions substantially increased photoactivity for the degradation of CHCl<sub>3</sub> under UV irradiation, whereas doping with Co<sup>3+</sup> and Al<sup>3+</sup> decreased photoactivity. The relative photocatalytic efficiency of a metal-ion dopant depends on whether it serves as a mediator of interfacial charge transfer or as a recombination center. Chen et al.<sup>22</sup> also showed that Fe- or Ni-doped TiO<sub>2</sub> has higher photoactivities than undoped TiO<sub>2</sub> under UV irradiation.

Numerous metal ions have been investigated as potential dopants including iron,<sup>1–3</sup> nickel,<sup>4,5</sup> vanadium,<sup>6–8</sup> chromium,<sup>9–11</sup> platinum,<sup>24</sup> ruthenium,<sup>25</sup> and cobalt ions.<sup>26,27</sup> However, there are conflicting results on the effects of doping on the visible-light photoactivity of TiO<sub>2</sub>. The wide variability in reported impact on visible-light activity may be due to the specific preparation methods, the actual photolysis and experimental conditions used to quantify activity, and the broad array of chemical reactions used to verify photoactivity over a broad range of wavelengths at  $\lambda > 400$  nm. For example, metal-ion-doped TiO<sub>2</sub> is prepared in the form of powders<sup>2,25,27</sup> and films<sup>6,7</sup> by different synthetic methods such as sol–gel syntheses<sup>6,8,11</sup> MOCVD,<sup>1</sup> hydrothermal synthesis,<sup>3</sup> solid-state reactions,<sup>4</sup> and ion implantation.<sup>10,28</sup> Photoactivity in the visible has been quantified using a wide array of substrates including dyes,<sup>1,3,6,8,11</sup> phenolic compounds,<sup>2,24,29</sup> acetaldehyde,<sup>6,27</sup> and nitric oxide.<sup>10,28</sup> Therefore, it is difficult to compare the net effects of metal-ion dopants on the photocatalytic activity of TiO<sub>2</sub>. Several reports<sup>30–32</sup> compare the effects of metal-ion dopants on visible-light photocatalytic activities of TiO<sub>2</sub> using high-throughput (HT) screening techniques. However, the physicochemical properties of various doped TiO<sub>2</sub> samples were not made in such combinatorial approaches.

We now report on the synthesis of sol–gel TiO<sub>2</sub> doped with 13 different metal ions and compare the effects of individual dopants on the resulting physicochemical properties (e.g., a crystal structure and UV–vis absorption) and their corresponding photocatalytic activities with respect to the catalysis of several reactions under visible-light irradiation ( $\lambda > 400$  nm). In this regard, the photocatalytic activities of metal-ion-doped TiO<sub>2</sub> are quantified in terms of the photobleaching of methylene

\* To whom correspondence should be addressed. Telephone: +1 626 395 4391. E-mail: mrh@caltech.edu.

<sup>†</sup> California Institute of Technology.

<sup>‡</sup> Kyungpook National University.

blue (MB), the oxidation of iodide ( $I^-$ ), and the degradation of phenol in aqueous suspensions.

## Experimental Details

**Chemicals.** The specific reagents used in this study include the following: titanium tetraisopropoxide (TTIP, Aldrich), absolute ethanol (Mallinckrodt), nitric acid ( $HNO_3$ , Aldrich), methylene blue (MB, J. T. Baker), potassium iodide (KI, EM Science), and phenol (Mallinckrodt). The metal-ion salts used in the preparations include the following:  $AgNO_3$  (Mallinckrodt),  $Cu(NO_3)_2 \cdot 4H_2O$  (Alfar Aesar),  $Ni(NO_3)_2 \cdot 6H_2O$  (Alfar Aesar),  $Cr(NO_3)_3 \cdot 9H_2O$  (Adrich),  $CrO_3$  (Aldrich),  $CoCl_2$  (Aldrich),  $VCl_3$  (Aldrich),  $RuCl_3$  (Aldrich),  $FeCl_3 \cdot 6H_2O$  (Aldrich),  $YCl_3 \cdot 6H_2O$  (Aldrich),  $LaCl_3 \cdot 7H_2O$  (Aldrich),  $OsCl_3$  (Aldrich),  $PtCl_4$  (Aldrich),  $Pt(NH_3)_4(NO_3)_2$  (Alfar Aesar), and  $RbClO_4$  (MP Biomedicals Inc.).

**Synthesis and Characterization of Catalysts.**  $TiO_2$  nanoparticles were prepared by standard sol–gel methods.  $TiO_2$  sols were prepared by dropwise addition of 5 mL of an ethanolic TTIP solution, which had been dissolved in 50 mL of absolute ethanol, into 50 mL of distilled water adjusted to pH 1.5 with nitric acid under vigorous stirring at room temperature. After continuously stirring for 24 h, the resulting transparent solution was evaporated using a rotary evaporator at 45 °C and dried in the oven (70 °C) overnight. The obtained powder was calcined at various temperatures from 200 to 700 °C (typically at 400 °C) for 1 h under air. Metal-ion-doped  $TiO_2$  samples (M- $TiO_2$ ) were prepared according to the above procedure in the presence of the corresponding metal-ion salt precursors to give a doping level from 0.1 to 1.0 atomic % (at. %). The appropriate amount of metal-ion precursor was added to the distilled water before hydrolysis of TTIP, and the remaining procedures were the same as described above. The doped  $TiO_2$  products exhibited a variety of different colors. Doping with  $Cr^{3+}$ ,  $Cu^{2+}$ , and  $Ni^{2+}$  produced  $TiO_2$  samples with a green color.  $Os^{3+}$ ,  $Pt^{4+}$ , and  $Pt^{2+}$  doping produced brown products,  $Ru^{3+}$  doping yielded a dark brown product;  $V^{3+}$  doping produced an orange product,  $Fe^{3+}$  doping produced a light orange product, and  $Co^{2+}$  doping gave a light yellow  $TiO_2$  product. All the other metal-doped samples are white colored.

Crystal structure patterns of the M- $TiO_2$  powder samples were examined by X-ray diffraction (XRD) using a Philips diffractometer (X'pert Pro) with Cu K $\alpha$  radiation. Brunauer–Emmett–Teller (BET) surface area measurement were carried out by using  $N_2$  as the adsorptive gas (Micromeritics Gemini), and the morphology and elemental composition analysis were performed by scanning electron microscopy (SEM, LEO 1550 VP) equipped with EDS (energy dispersive X-ray spectroscopy). UV–vis diffuse reflectance spectra (DRS) were obtained on a Shimadzu UV-2101PC spectrophotometer.

**Determination of Photocatalytic Activity.** The photocatalytic activities of the array of synthesized  $TiO_2$  samples were quantified by measuring the rates of photobleaching and degradation of MB, the rates of  $I^-$  oxidation, and the rates of degradation of phenol. Synthesized  $TiO_2$  samples were dispersed in distilled water (1 g  $L^{-1}$ ). This was followed by the addition of an aliquot of substrate stock solution to the catalyst suspension to obtain a specific substrate concentration (i.e.,  $[MB]_0 = 10 \mu M$ ,  $[I^-]_0 = 50 \text{ mM}$ , and  $[PhOH]_0 = 50 \mu M$ ). The reaction suspensions pH were circum-neutral at  $t = 0$ . Before irradiation, the suspension was stirred in the dark for 30 min to obtain a state of sorption equilibrium of the specific substrate on  $TiO_2$ . A high-pressure Hg(Xe) arc lamp (500 W) was used as the light source. The incident light beam was passed through an IR water

filter and a UV cutoff filter giving  $\lambda > 320 \text{ nm}$  for UV irradiation or  $\lambda > 400 \text{ nm}$  for visible irradiation before being focused onto a cylindrical Pyrex reactor through a quartz window. The reactor was open to ambient laboratory air during photolysis with a few exceptions. Time-sequenced sample aliquots were collected from the reactor during the time course of illumination for analysis and filtered through a 0.45  $\mu m$  PTFE syringe filter to remove  $TiO_2$  particles. Multiple photolysis experiments were performed under the identical reaction conditions to determine reproducibility.

The rate constants for the observed degradation of MB during photolysis were determined by measuring the absorbance of sample aliquots at 665 nm with a conventional spectrophotometer. In the case of the photocatalytic oxidation of iodide, tri-iodide ion ( $I_3^-$ ), which is the principal product of iodide oxidation in the presence of excess iodide ion, was determined spectrophotometrically by measuring its absorbance at 352 nm. The degradation of phenol in aqueous solution was measured using high-performance liquid chromatography (HPLC, HP 1100 series with a C18 column).

## Results and Discussion

**X-ray Diffraction Analysis of Metal-Ion-Doped  $TiO_2$  (M- $TiO_2$ ).** The structure of  $TiO_2$  samples that were synthesized by standard sol–gel methods appeared to be amorphous; however, postsynthesis treatment by thermal annealing at various temperatures ranging from 200 to 700 °C resulted in higher degrees of crystallinity with anatase as the principal phase. The increasing calcination temperatures resulted in an increase in the intensity and sharpness of the anatase peaks. This trend is clearly indicative of an improvement in the degree of crystallinity corresponding to the formation of larger particles with fewer defects. However, above a given temperature, XRD peaks corresponding to the rutile phase appear. No obvious diffraction peaks that could be attributed to the metal-ion dopants were observed. Thus, the crystal structure of  $TiO_2$  indicates a mixture of anatase and rutile for all the synthesized M- $TiO_2$  samples. These results suggest that the doping levels that were employed or the subsequent thermal treatments did not induce the formation of discrete impurity phases. Furthermore, the metal ions appear to have been fully integrated into the basic structure of  $TiO_2$ . However, it is conceivable that metal impurities, which were formed during synthesis, were nanoscopic or possibly dispersed on the surface. We have assumed that some of the metal-ion dopants such as  $Pt^{4+}$ ,  $Cr^{3+}$ , and  $V^{3+}$  ions are most likely substituted in  $Ti^{4+}$  sites within  $TiO_2$  because the ionic radii of the dopants ( $Pt^{4+}$ , 0.765 Å;  $Cr^{3+}$ , 0.755 Å;  $V^{3+}$ , 0.78 Å) are similar to that of  $Ti^{4+}$  (0.745 Å). In contrast, metal-ion dopants such as  $Co^{2+}$ ,  $Cu^{2+}$ , and  $Pt^{2+}$  ions are most likely located in interstitial positions of the lattice rather than directly in  $Ti^{4+}$  sites because of the relatively large size difference between dopant ions ( $Co^{2+}$ , 0.89 Å;  $Cu^{2+}$ , 0.87 Å;  $Pt^{2+}$ , 0.94 Å) and  $Ti^{4+}$ . However,  $Ag^+$ ,  $Rb^+$ ,  $Y^{3+}$ , and  $La^{3+}$  ions seem to be too large to be incorporated in the  $TiO_2$  lattice, and thus, they are more likely to be found as dispersed metal oxides within the crystal matrix or dispersed on the surface of  $TiO_2$ .

The anatase-to-rutile phase transformation (i.e., the A–R phase transformation) of pure  $TiO_2$  normally occurs between 600 and 700 °C.<sup>33–36</sup> Pure (undoped)  $TiO_2$  samples that were calcined at 400 °C showed only the anatase phase. Calcination at 700 °C produced a relatively small fraction of the rutile phase. However, it was observed that, in some cases, metal-ion doping altered the temperature of the A–R phase transformation of  $TiO_2$ . In this regard, the XRD patterns of representative M- $TiO_2$

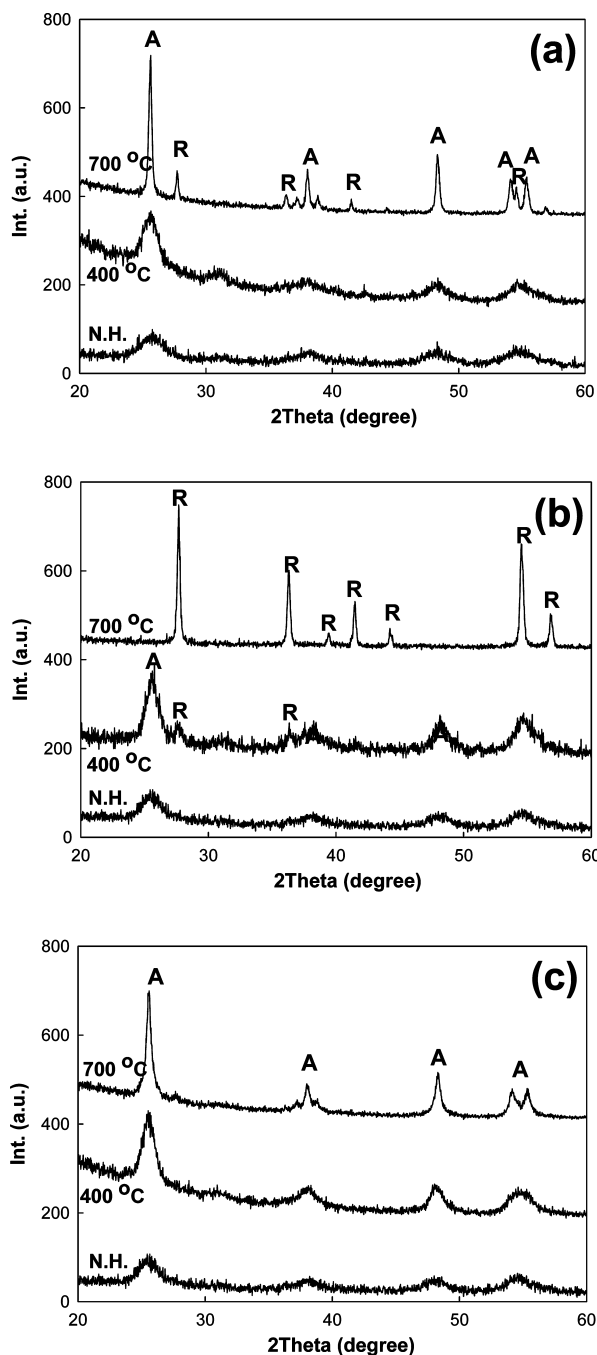


**Figure 1.** X-ray diffraction pattern measured for (a) 0.3 at. % La-TiO<sub>2</sub>, (b) 0.3 at. % Pt-TiO<sub>2</sub>, and (c) 0.3 at. % Ru-TiO<sub>2</sub> with various calcination temperatures (at 700, 400 °C and no heat treatment).

samples that were calcined at different temperatures are shown in Figure 1. Similar to undoped TiO<sub>2</sub>, La-TiO<sub>2</sub> prepared at 400 °C was entirely in the anatase phase. Anatase remained as the dominant phase until a minor rutile component was observed at 700 °C (Figure 1a). However, in the case of Pt-TiO<sub>2</sub>, a rutile peak at  $2\theta = 27.5^\circ$  appeared at 400 °C as shown in Figure 1b. This rutile peak was clearly dominant at 700 °C, while the anatase peak at  $2\theta = 25.7^\circ$  disappeared at 700 °C. In comparison, Ru-TiO<sub>2</sub> was to be almost exclusively as pure anatase phase even at 700 °C in Figure 1c, implying that Ru ion inhibited A–R phase transformation of TiO<sub>2</sub>.

In order to compare the effects of metal-ion doping on the A–R phase transformation, the fraction of rutile,  $X_R$ , was calculated from the respective peak intensities using following equation<sup>37</sup>

$$X_R(\%) = \{1 - (1 + 1.26I_R/I_A)^{-1}\} \times 100 \quad (1)$$

where  $I_R$  and  $I_A$  are the X-ray intensities of the rutile (101) and anatase (110) peaks, respectively. These relative rutile fractions are listed in Table 1 with ionic radii of the dopants. Pt-TiO<sub>2</sub>, Cr-, V-, Fe-, Y-, and Rb-TiO<sub>2</sub> also exhibited evidence of a rutile phase after calcinations at 400 °C.

The relative rutile fractions were estimated to be in the range of 15–30%, whereas the undoped samples and remaining M-TiO<sub>2</sub> samples were in the pure anatase phase. Pt- and Y-TiO<sub>2</sub>, which were calcined at 700 °C, also exhibited high rutile fractions ( $X_R = 100\%$  and 62%, respectively) when compared to undoped TiO<sub>2</sub> ( $X_R = 15\%$ ). Therefore, we conclude that some of the dopants (e.g., Pt, Cr, V, Fe, Y, and Rb) lowered the A–R phase transformation temperature of TiO<sub>2</sub>. In the specific case of Ru-TiO<sub>2</sub> calcined at 700 °C, the  $X_R$  fraction was estimated to be only 3%, which indicates that Ru increased the apparent temperature of A–R phase transformation. Similar results have been reported elsewhere.<sup>1,38–42</sup>

However, some previous studies reported controversial results of doping effect on A–R phase transformation. For example, Ruiz et al.<sup>43</sup> reported that Cr-TiO<sub>2</sub> inhibited the A–R phase transformation. However, they observed an additional XRD peak due to Cr<sub>2</sub>O<sub>3</sub> as well as TiO<sub>2</sub>. The formation of chromium oxide is most likely due to the high doping level of Cr at 5–10 at. %. In comparison, no Cr-related peaks were observed at our doping level of Cr (0.3 at. %). Therefore, it is likely that an effect of doping on A–R phase transformation temperature depends on the actual doping concentration. Doping at high Cr ion concentrations, which may result in Cr segregated on TiO<sub>2</sub> surface as opposed to direct substitution in Ti<sup>4+</sup>, may impact the A–R phase transformation differently. Some studies also showed that doping with Ce, La, or Y ions also inhibits the

**TABLE 1:** Ionic Radii of Dopants, Rutile Content by XRD, Surface Area, and Color of Various Metal-Ion-Doped TiO<sub>2</sub> Nanoparticles (at 0.3 at. % Doping)

dopant	ionic radius <sup>a</sup> (Å)	rutile (%)	surface area (m <sup>2</sup> g <sup>-1</sup> )	color <sup>d</sup>
@ 400 °C calcination				
undoped TiO <sub>2</sub>	0.745	0	104	white
Pt(II)	0.940	22	111	light brown
Pt(IV)	0.765	26	106	light brown
Cr(III)	0.755	34	115	green
Cr(VI)	0.580	29	125	green
V(III)	0.780	13	132	orange
Ru(III)	0.820	0	112	dark brown
Ni(II)	0.830	0	112	green
Fe(III)	0.785 <sup>b</sup>	13	113	light orange
Co(II)	0.885 <sup>b</sup>	0	102	light yellow
Cu(II)	0.870	0	110	light green
Os(III)	0.770 <sup>c</sup>	0	117	light brown
Ag(I)	1.290	0	117	white
Rb(I)	1.660	19	108	white
Y(III)	1.040	18	121	white
La(III)	1.170	0	132	white
@ 700 °C calcination				
undoped TiO <sub>2</sub>		15		
Pt(II)		100		
Y(III)		62		
La(III)		18		
Ru(III)		3		

<sup>a</sup> From literature: Shannon, R. D. *Acta Crystallogr., Sect. A* **1976**, 32, 751. <sup>b</sup> Values for high spin in literature (a). <sup>c</sup> Value for Os (IV); no available value for Os (III) in literature (a). <sup>d</sup> With samples before heat treatment.

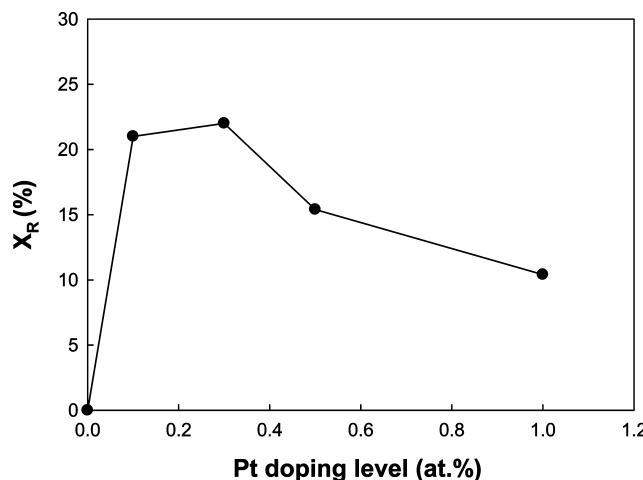


**Figure 2.** Fraction of rutile (%) as a function of doping level of Pt(II) in  $\text{TiO}_2$  (at. %). Samples have been prepared by the sol-gel method and calcined at 400 °C for 1 h.

A-R phase transformation.<sup>34,38,44</sup> The inhibition by these dopants has been explained in terms of the formation of  $\text{Ti}-\text{O}-\text{Ce}$  (or La, Y) bonds at the interface, since they could be located primarily on the surface of  $\text{TiO}_2$  because of the relatively large differences in the ionic radii resulting in inhibited crystal grain growth.<sup>45,46</sup> A similar inhibition of A-R phase transformation has been pointed out for  $\text{TiO}_2/\text{SiO}_2$  mixture as well.<sup>33,36</sup> However, our results indicate that La doping had little impact on the A-R phase transformation, while Y accelerated the transformation. It should be noted that the doping levels of La, Y, and Ce ions in  $\text{TiO}_2$  are about 5–10 at. % in most studies in contrast to a level of 0.3 at. % in this study. In addition, Ghosh et al.<sup>38</sup> showed that peaks due to  $\text{Y}_2\text{Ti}_2\text{O}_7$  or  $\text{La}_4\text{Ti}_9\text{O}_{24}$  were identified in the XRD patterns of Y- or La-doped  $\text{TiO}_2$  samples that showed an inhibiting effect on the A-R phase transformation, whereas no Y- or La-derived peaks were observed in our XRD results.

In order to investigate the effect of the doping level concentration on the A-R phase transformation, the fractions of rutile ( $X_R$ ) in Pt(II)- $\text{TiO}_2$  with different Pt concentration from 0.1 to 1.0 at. % were determined. As shown in Figure 2,  $X_R$  fraction increases to approximately 22% when Pt is doped in the range of 0.1–0.3 at. % and then decreases at higher doping levels in the range of 0.5–1.0 at. %. These results indicate that the doping effect of metal ions on the A-R phase transformation is dependent on the intrinsic physicochemical properties of the doping metal ion but also on the specific concentration of the individual dopants. Shannon et al.<sup>47</sup> also reported that the total impurity level can affect the transformation through the structure stuffing effect. In addition, they also reported that large quantities of impurities may raise the transformation temperatures.

There are only a few concepts or rules to clarify the effects of impurities doped into  $\text{TiO}_2$  on the A-R phase transformation. The primary factor that has been invoked in order to explain the doping effect on A-R phase transformation is the creation of oxygen vacancies since the A-R phase transformation involves a contraction or shrinking of the oxygen structure.<sup>47</sup> It is also believed that impurities can affect the rate of the transformation by modifying the defect structures of  $\text{TiO}_2$ . Based on this concept, Shannon et al.<sup>47</sup> suggested that processes that increase oxygen vacancies, such as the addition of ions of valence less than four and of small ionic radius which can enter the structure via direct substitution, accelerate the A-R phase transformation (and vice versa). They also hypothesized that

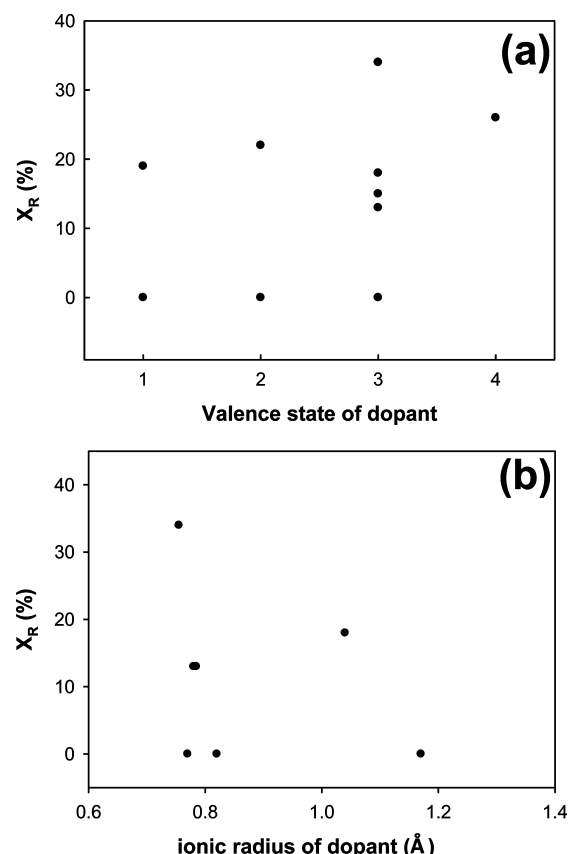


**Figure 3.** Fraction of rutile phase (%) in M- $\text{TiO}_2$  as a function of (a) valence state of dopant and (b) ionic radius of trivalent ion dopants.

an increase of oxygen vacancy concentration reduces the strain energy that must be overcome before the rearrangement of octahedral  $\text{Ti}-\text{O}$  occurs. In addition, Mackenzie et al.<sup>48</sup> proposed a rank-ordered list of dopants in terms of their effectiveness in accelerating the A-R phase transformation and concluded that monovalent ions are more effective than divalent or trivalent ions since more oxygen vacancies would be created in the doping of monovalent ions compared to divalent or trivalent ions.

According to our results, however, there is no such a correlation observed between the valence state of dopant and the fraction of rutile phase of M- $\text{TiO}_2$ . For example, the fractions of the rutile phase of Pt(IV)- $\text{TiO}_2$  and Cr(III)- $\text{TiO}_2$  are compared to Pt(II)- $\text{TiO}_2$  and Cr(VI)- $\text{TiO}_2$  in Table 1. The doping with Pt(IV) ion also accelerated the A-R phase transformation with the fraction of rutile from 0% to 26%, and it was similar to rutile fraction of Pt(II)- $\text{TiO}_2$  sample (22%). With respect to Cr doping, both Cr(VI) and Cr(III) accelerated the A-R phase transformation as well. In addition, the data as shown in Figure 3 demonstrates that there are no obvious correlations between  $X_R$  in various M- $\text{TiO}_2$  samples as a function of valence state or ionic radius of each metal dopant. Figure 3a also shows that the doping with monovalent ions was not more effective in terms of the A-R phase transformation than divalent or trivalent ions and that the fraction of rutile varied even with same valence state of dopant ions. Figure 3b also shows the  $X_R$  fraction of the trivalent ion-doped  $\text{TiO}_2$  samples as a function of their ionic radii; it is clear from this plot that there is no correlation. Therefore, the valence state or ionic radius of dopant metal ion is not a good predictor of the effectiveness of specific dopants on the A-R phase transformation even if oxygen vacancies, which might be induced by metal-ion doping, affect the A-R phase transformation of M- $\text{TiO}_2$  samples.

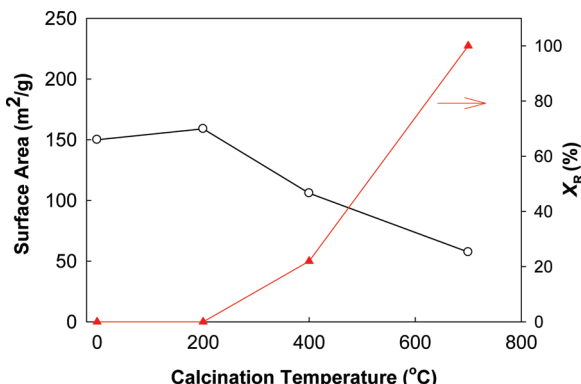


**Figure 4.** BET surface area and the fraction of rutile ( $X_R$ ) of 0.3 at. % Pt-TiO<sub>2</sub> as function of calcination temperature.

**BET Surface Areas and SEM Characterization.** BET surface areas (Table 1) were determined using nitrogen adsorption and desorption isotherms. The BET surface area of the unadulterated sol–gel synthesized TiO<sub>2</sub>, which was calcined at 400 °C, was determined to be 104 m<sup>2</sup> g<sup>-1</sup>. In comparison, the surface area of the commercial product, Degussa P25 TiO<sub>2</sub>, is listed at 50 m<sup>2</sup> g<sup>-1</sup> and confirmed by our measurements. The BET surface areas of the M-TiO<sub>2</sub> samples were found to be slightly larger than the undoped TiO<sub>2</sub> (110–130 m<sup>2</sup> g<sup>-1</sup> for M-TiO<sub>2</sub> samples). Figure 4 shows the change of BET surface areas and rutile fractions of 0.3 at. % Pt(II)-TiO<sub>2</sub> as a function of calcination temperature. The BET surface area of Pt(II)-TiO<sub>2</sub> is  $\sim$ 150 m<sup>2</sup> g<sup>-1</sup> without heat treatment and at 200 °C calcination. Calcination at 400 °C decreases the observed surface area as the rutile phase appears. At 700 °C, where Pt-TiO<sub>2</sub> is found in the pure rutile phase, the surface area decreased to 57 m<sup>2</sup> g<sup>-1</sup>.

The SEM images of Pt-TiO<sub>2</sub> and Cr-TiO<sub>2</sub> particles, which are shown in Figure 5, show that the particles are highly aggregated and surfaces are clearly rough. In addition, the characteristic particle sizes become larger at higher calcination temperatures with a corresponding decrease in surface area. Images of other M-TiO<sub>2</sub> samples (which are not shown here) were similar to Pt-TiO<sub>2</sub> (or Cr-TiO<sub>2</sub>).

The elemental composition of the various M-TiO<sub>2</sub> samples was estimated by EDS. The EDS spectra of most of M-TiO<sub>2</sub> samples including TiO<sub>2</sub> doped with Pt<sup>2+</sup> and Ni<sup>2+</sup> ions (relatively larger ionic radii of metal dopants) showed no apparent signals directly related to metal dopants. These results indicate that these metal ions are well incorporated into TiO<sub>2</sub> lattice (possibly interstitials of TiO<sub>2</sub> in the case of Pt-TiO<sub>2</sub> or Ni-TiO<sub>2</sub>) and not located on or near the surface of the particles. On the other hand, the EDS spectra of the larger ionic radii dopants (M-TiO<sub>2</sub>) such as Ag-TiO<sub>2</sub> and Rb-TiO<sub>2</sub> clearly showed signals for the metal ions, which indicates that these metal-ion dopants (i.e., Ag, Rb, Y, and La) are located near the surface region and that they are not incorporated into the TiO<sub>2</sub> lattice due to their substantially larger ionic radii compared to Ti<sup>4+</sup> (see Supporting Information, Figure S1).

**UV–Vis Diffuse Reflectance Spectra.** The UV–vis diffuse reflectance spectra of the array of metal-ion-doped TiO<sub>2</sub> samples are shown in Figure 6. The sol–gel synthesized, undoped TiO<sub>2</sub> (TiO<sub>2</sub>–SG) and Degussa P25 TiO<sub>2</sub> are characterized by sharp absorption edges at about 400 nm ( $E_{bg} \sim 3.1$  eV). However, most of M-TiO<sub>2</sub> samples show extended absorption spectra into the visible region over the range of 400–700 nm. Figure 6a shows that TiO<sub>2</sub> samples doped with Fe, Cu, and Ni ions exhibited relatively small absorption between 400 and 550 nm, while Co-, Os-, V-, Ru-, or Cr-doped TiO<sub>2</sub> samples showed

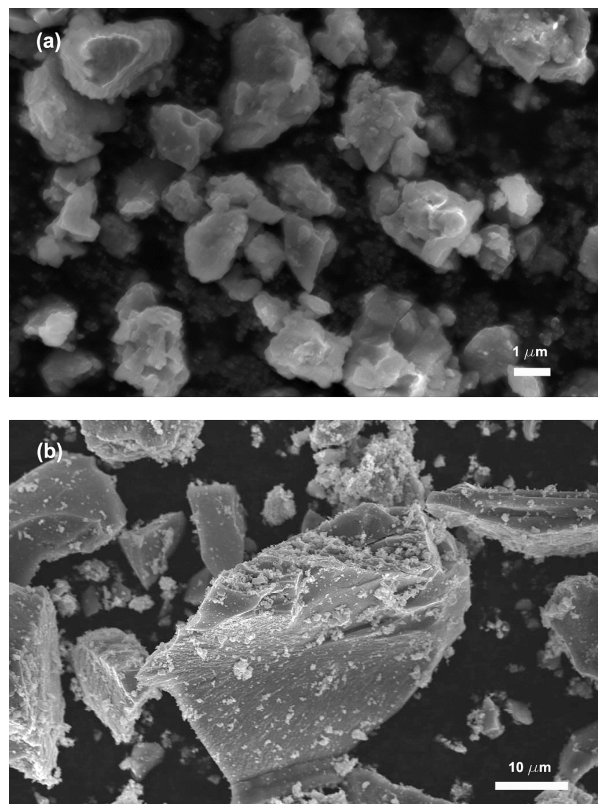


**Figure 5.** SEM images of (a) 0.3 at. % Pt-TiO<sub>2</sub> and (b) 0.3 at. % Cr-TiO<sub>2</sub> synthesized by the sol–gel method with 400 °C calcination.

substantial and broader absorption shoulders up to 700 nm (Figure 6b). Figure 6c illustrates the difference between the absorption spectra of Pt(IV)-TiO<sub>2</sub> and Pt(II)-TiO<sub>2</sub>. Pt(II)-TiO<sub>2</sub> shows a much broader absorption over most of the visible region similar to V-TiO<sub>2</sub> (Figure 6b). However, Pt(IV)-TiO<sub>2</sub> has a smaller absorption peak between 400 and 550 nm.

The extended absorption of the M-TiO<sub>2</sub> samples into the visible region has been explained in terms of the excitation of electrons from the dopant ions to the conduction band of TiO<sub>2</sub> (i.e., a metal to conduction band charge transfer). For example, the enhanced absorption observed for the M-TiO<sub>2</sub> samples doped with Fe, Cr, V, Co, Ni, and Cu in the visible region can be considered to involve excitation of 3d electrons of the dopant ion to the conduction band according to their respective energy levels.<sup>2,3,6,7,49–51</sup> However, the absorption spectra of modified TiO<sub>2</sub> in the visible region may originate from defects associated with oxygen vacancies that give rise to colored centers.<sup>52,53</sup> Kuznetsov and Serpone pointed out the similarities of the spectra in the range of 400–600 nm shown among different types of visible-light-active TiO<sub>2</sub> samples, and these similarities were found even in reduced TiO<sub>2</sub> samples.<sup>52,54,55</sup> They also observed that the absorption spectra were given by the sum of overlapping absorption bands with maxima at 2.81 and 2.55 eV, which correlate with oxygen vacancies.<sup>52,53</sup> In fact, the metal-ion dopants used in this study have different valence states than Ti<sup>4+</sup> and, as a consequence, may induce the generation of oxygen vacancies during synthesis. In addition, similarities of the absorption spectra in the range of 400–600 nm that Kuznetsov et al. observed were also found among several M-TiO<sub>2</sub> samples in this study even though the absorption intensities were different. Therefore, the generation of new energy levels due to the injection of impurities within the band gap coupled with the generation of oxygen vacancies by metal-

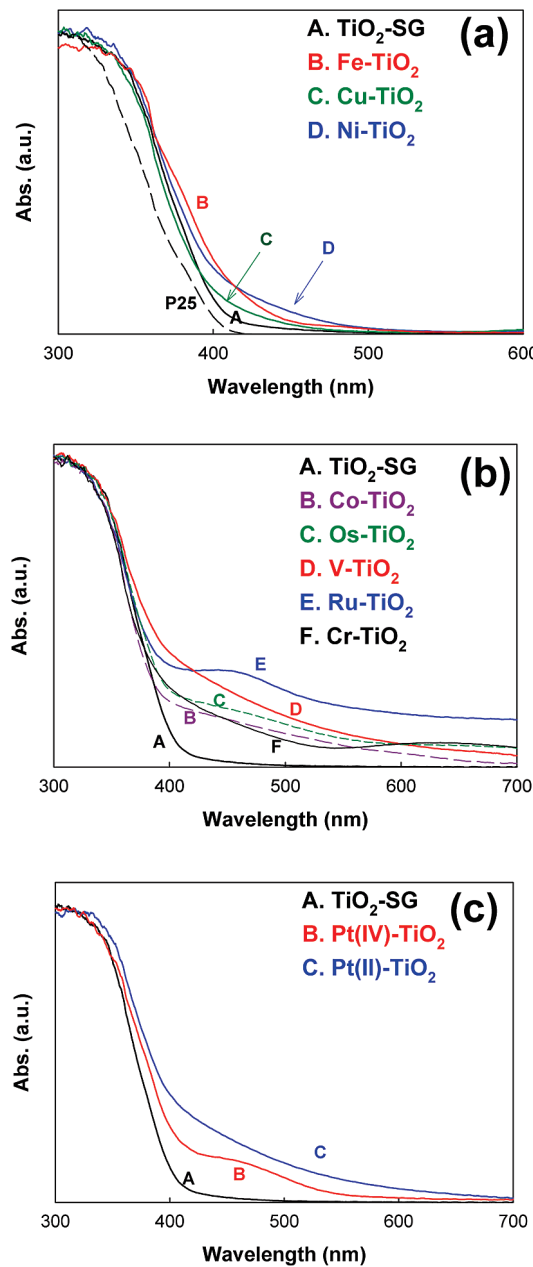


**Figure 6.** UV-vis diffuse reflectance spectra (DRS) for various M-TiO<sub>2</sub> samples (0.3 at. % doping). Absorption spectra for Ag-, Rb-, Y-, and La-TiO<sub>2</sub> samples, which are not shown here, are identical with that of undoped TiO<sub>2</sub>.

ion doping may contribute to the observed visible-light absorption of the M-TiO<sub>2</sub> samples. We find that there are no visible-light extended absorption spectra for M-TiO<sub>2</sub> with Ag-, Rb-, Y-, and La-TiO<sub>2</sub>, which is consistent with this hypothesis. As discussed above, the ionic radii of these dopants are too large to be readily substituted for Ti<sup>4+</sup> in the lattice of TiO<sub>2</sub>. Thus, they are considered to be dispersed on the surface of TiO<sub>2</sub> particles. This interpretation is consistent with the results of the EDS analysis (see Supporting Information, Figure S1).

**Visible-Light Photocatalytic Activities of M-TiO<sub>2</sub>.** The photobleaching and degradation of MB under visible-light irradiation follows apparent first-order kinetics. The observed reaction rate constants ( $k_{MB}$ ) with the various M-TiO<sub>2</sub>, which are prepared at a doping level of 0.3 at. % and calcined at 400 °C under both UV and visible-light irradiation, are listed in Table 2. Under visible-light irradiation at  $\lambda > 400$  nm,  $k_{MB}$  for direct photolysis without TiO<sub>2</sub> particles is estimated to be 0.003 min<sup>-1</sup>.

**TABLE 2: Visible-Light Photocatalytic Activities of Various M-TiO<sub>2</sub> Samples for the Degradation of Methylene Blue (MB), the Oxidation of Iodide (I<sup>-</sup>), and the Degradation of Phenol (PhOH)**

dopant	$k_{MB}$ (min <sup>-1</sup> )		$[I_3^-]_{prod,15min}$ (μM)		$k_{PhOH}$ (h <sup>-1</sup> )
	vis	UV	vis	UV	
direct photolysis	0.003	0.011	0	0	0
undoped TiO <sub>2</sub>	0.005	0.014	10	24	0.09
Pt(II)	0.014	0.053	19	40	0.80
Pt(IV)	0.013	0.057	32	42	1.29
Cr(III)	0.013	0.016	27	25	0.36
V(III)	0.012	0.015	16	21	0.13
Ni(II)	0.011	0.010	15	27	0.09
Ru(III)	0.005	0.007	8		0.07
Fe(III)	0.007	0.015	12		0.10
Cu(II)	0.009	0.016	8		0.08
Co(II)	0.009	0.015	12		0.11
Os(III)	0.009	0.013	12		0.09
Ag(I)	0.008	0.016	12		0.07
Rb(I)	0.011	0.033	12		0.07
Y(III)	0.007	0.018	9		0.08
La(III)	0.005	0.016	10		0.10

The observed rate constant was increased slightly to 0.005 min<sup>-1</sup> in the presence of undoped TiO<sub>2</sub>. This activity may be due to additional light absorption above 400 nm of TiO<sub>2</sub> particles or enhanced direct electron injection from adsorbed MB to the conduction band of TiO<sub>2</sub>. However, Pt-, Cr-, V-, Ni-, and Rb-TiO<sub>2</sub> showed significantly enhanced photocatalytic activities under the visible-light irradiation by an order of magnitude ( $k_{MB} > 0.01$  min<sup>-1</sup>). Among all tested M-TiO<sub>2</sub> samples, Pt-TiO<sub>2</sub> (both Pt(II)-TiO<sub>2</sub> and Pt(IV)-TiO<sub>2</sub>) showed the best visible-light photoactivity for MB degradation. Most of the other M-TiO<sub>2</sub> samples (i.e., Fe-, Co-, Cu-, Os-, Ag-, and Y-TiO<sub>2</sub>) showed slightly increased  $k_{MB}$ , while Ru- and La-TiO<sub>2</sub> had negligible effect when compared to undoped TiO<sub>2</sub>. None of the M-TiO<sub>2</sub> samples had lower photocatalytic activities when compared to the undoped SG-TiO<sub>2</sub>. Under UV irradiation (>320 nm), Pt-TiO<sub>2</sub> and Rb-TiO<sub>2</sub> had significantly enhanced photocatalytic activities for MB degradation as well. However, Cr- and V-TiO<sub>2</sub>, which had comparable  $k_{MB}$  values to Pt-TiO<sub>2</sub> under visible-light irradiation, had slightly enhanced photocatalytic activities under UV irradiation.

In some cases, the rates of degradation of MB were increased even with several M-TiO<sub>2</sub> samples that did not show extended visible-light absorption. For example, Rb-TiO<sub>2</sub>, which has the same absorption spectrum as undoped TiO<sub>2</sub>, gave a higher  $k_{MB}$  value than undoped TiO<sub>2</sub> under visible-light irradiation. In a similar fashion, Ag- and Y-TiO<sub>2</sub> also showed slightly enhanced visible-light photocatalytic activities. Therefore, the enhanced photocatalytic activities of Rb-, Ag-, and Y-TiO<sub>2</sub> for MB degradation were not attributed to efficient utilization of visible light with M-TiO<sub>2</sub>. It might be due to other effects of dopants located on the surface of TiO<sub>2</sub> such as enhanced photoinduced charge transfer due to visible-light absorption by the surface-bound MB. Therefore, it appears that MB is not an appropriate model compound to evaluate the relative photocatalytic activities of visible-light photocatalysts (i.e., modified TiO<sub>2</sub>). Yan et al.<sup>56</sup> also reported that the photoaction spectrum for photocatalytic degradation of MB under visible-light irradiation is similar to the photoabsorption spectrum of the dye, which supports their suggestion that the MB molecules directly absorb photons, and thus the photoexcited electrons may be injected into the underlying M-TiO<sub>2</sub>. However, some studies only showed extended absorption of modified photocatalysts into the visible range and enhanced degradation rates of dyes as compared to

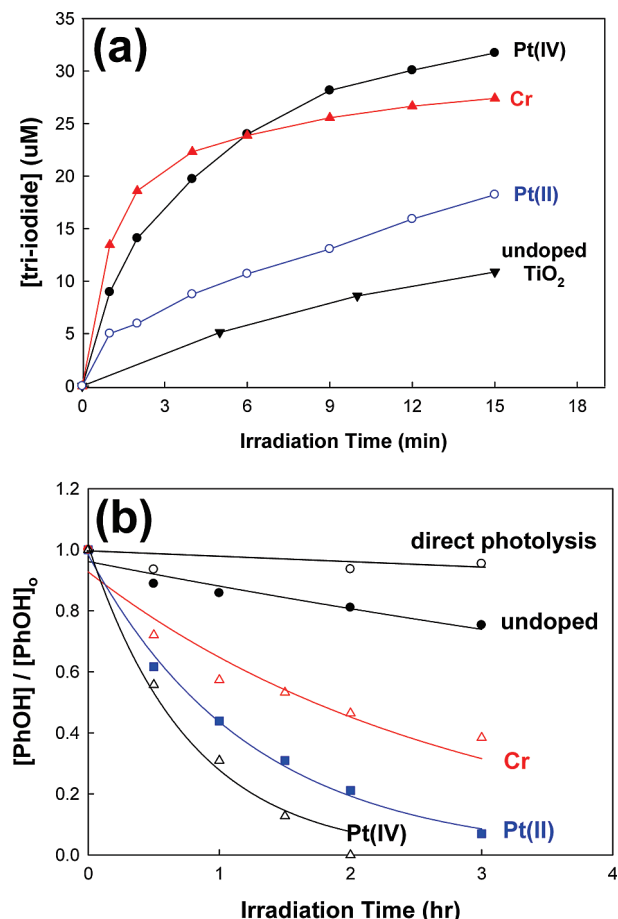
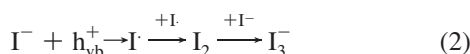


**Figure 7.** Visible-light photocatalytic activities of 0.3 at. % Pt-TiO<sub>2</sub> and 0.3 at. % Cr-TiO<sub>2</sub>: (a) the production of tri-iodide by iodide oxidation with [I<sup>-</sup>]<sub>0</sub> = 50 mM, (b) the degradation of phenol with [phenol]<sub>0</sub> = 50 μM (total volume = 30 mL, 1 g/L suspension, 500 W,  $\lambda > 400$  nm).

unmodified ones and then concluded that their modified photocatalysts have intrinsic visible-light photoactivities.<sup>3,8,15,16,57,58</sup>

Iodide is oxidized readily by valence-band holes or surface-bound hydroxyl radical in aqueous solution to from tri-iodide (I<sub>3</sub><sup>-</sup>) according to the following reaction sequence:



The production of I<sub>3</sub><sup>-</sup> ions from I<sup>-</sup> oxidation during photolysis in the presence of Pt-TiO<sub>2</sub> and Cr-TiO<sub>2</sub> is shown in Figure 7a. No I<sub>3</sub><sup>-</sup> was produced in the absence of TiO<sub>2</sub> particles at  $\lambda > 400$  nm, and undoped TiO<sub>2</sub> showed little photocatalytic activity with respect to the net photooxidation of I<sup>-</sup> to I<sub>3</sub><sup>-</sup>. In contrast, Cr-TiO<sub>2</sub> and Pt(IV)-TiO<sub>2</sub> had significantly enhanced photocatalytic activities with respect to iodide oxidation. Unlike undoped TiO<sub>2</sub>, the production of I<sub>3</sub><sup>-</sup> with Cr-TiO<sub>2</sub> or Pt(IV)-TiO<sub>2</sub> occurred in a relatively fast initial period of irradiation followed by an approach to a steady state that may be due to the reduction of I<sub>3</sub><sup>-</sup> to I<sup>-</sup> by conduction band electrons (i.e., the rate of the back electron transfer reaction increases as the concentration of I<sub>3</sub><sup>-</sup> ions increases, and thus a steady state is achieved).

The comparative photocatalytic activities of the all M-TiO<sub>2</sub> samples are ranked in Table 2 in terms of the total amount of I<sub>3</sub><sup>-</sup> produced during 15 min of irradiation. Cr-TiO<sub>2</sub> and Pt(IV)-TiO<sub>2</sub> substantially enhanced the visible-light photocatalytic activity with respect to I<sup>-</sup> oxidation, while Pt(II)-, V-, and Ni-

TiO<sub>2</sub> are only slightly enhanced. In contrast, the other M-TiO<sub>2</sub> products exhibited negligible activity during the 15 min reaction time. Unlike the degradation reaction of MB, Ag-, Rb-, Y-, and La-TiO<sub>2</sub> exhibited no enhanced effects on visible-light activities with respect to I<sup>-</sup> oxidation.

The oxidations of iodide in suspensions of Pt-, Cr-, V-, and Ni-TiO<sub>2</sub>, which showed enhanced visible-light photocatalytic activities, were also investigated under UV irradiation at  $\lambda > 320$  nm. In the case of UV light illumination, Pt-TiO<sub>2</sub> had a higher photoactivity than undoped TiO<sub>2</sub>. However, the other M-TiO<sub>2</sub> materials showed almost the same photocatalytic activities as undoped TiO<sub>2</sub>. Pt(II)-TiO<sub>2</sub> had comparable photocatalytic activities to Pt(IV)-TiO<sub>2</sub> under UV irradiation, whereas it had lower photoactivity than Pt(IV)-TiO<sub>2</sub> under visible-light irradiation.

The photocatalytic degradation of phenol vs time in suspensions of Pt-TiO<sub>2</sub> and Cr-TiO<sub>2</sub> under visible-light irradiation is shown in Figure 7b. Pt(IV)-TiO<sub>2</sub> was also found to be the most effective photocatalyst for phenol degradation. Pt(II)-TiO<sub>2</sub> and Cr-TiO<sub>2</sub> also showed significantly enhanced visible-light photocatalytic activity, while V-TiO<sub>2</sub> had a moderately enhanced photoactivity (Table 2). The phenol degradation results were similar to those observed for I<sup>-</sup> oxidation. However, the other M-TiO<sub>2</sub> materials did not show any improvement in photocatalytic activities for phenol degradation under visible-light irradiation as shown in Table 2.

From our kinetics observations, we can conclude that the visible-light photocatalytic activities of the various M-TiO<sub>2</sub> materials are not directly correlated with their UV-vis absorption spectra. For example, Ru- and Os-TiO<sub>2</sub> did not have significant visible-light photocatalytic activities, even though they had extended absorption bands above 400 nm. V-TiO<sub>2</sub>, which has larger visible absorption than Cr- and Pt-TiO<sub>2</sub>, was found to be less active under visible-light illumination. The efficient absorption of visible light does not appear to be a decisive factor that determines the visible-light photocatalytic activity of M-TiO<sub>2</sub> although visible-light absorption is clearly necessary to initiate photoreactions. Moreover, visible-light photocatalytic activity of M-TiO<sub>2</sub> material also appears to be substrate-dependent. For MB degradation, most of the M-TiO<sub>2</sub> samples were found to have enhanced photocatalytic activities, although Pt-, Cr-, V-, Ni-, and Rb-TiO<sub>2</sub> were clearly the most efficient. The photo-oxidation rates of I<sup>-</sup> under visible-light irradiation were increased with Pt-, Cr-, V-, Ni-, and Fe-doped TiO<sub>2</sub> samples. However, only Pt-TiO<sub>2</sub> and Cr-TiO<sub>2</sub> showed significantly enhanced activities for the degradation of phenol. Therefore, it seems to be difficult to correlate visible-light photocatalytic activities with certain obvious physicochemical properties such as color, surface area, and light absorption of the M-TiO<sub>2</sub> materials as a function of the variation in M. However, it is interesting to note that visible-light photocatalytic activity was influenced by the fraction of rutile in M-TiO<sub>2</sub>. Pt-TiO<sub>2</sub>, and Cr-TiO<sub>2</sub>, which showed that the most enhanced visible-light photocatalytic activities for all tested reactions have higher fractions of rutile in TiO<sub>2</sub> as shown in Table 1. On the other hand, Ru-TiO<sub>2</sub> and Os-TiO<sub>2</sub> in the pure anatase phase did not show significantly enhanced visible-light photocatalytic activities for all reactions although they exhibited relatively large absorption in visible region of the spectrum. Even though Rb-TiO<sub>2</sub> and Y-TiO<sub>2</sub> had relatively high rutile content, no enhancement in visible-light photoactivity was observed since they had no measurable absorption in the visible region.

In order to investigate the effect of the fraction of rutile on visible-light photocatalytic activity, the photobleaching and

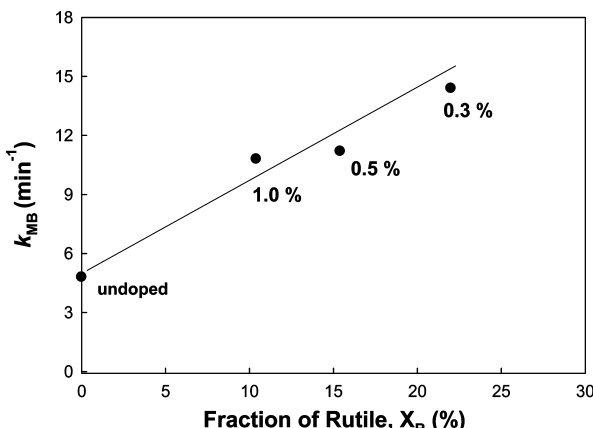


**Figure 8.** Correlation between photocatalytic activities for MB degradation (the degradation rate constant,  $k_{MB}$ ) at >400 nm irradiation and the fractions of rutile ( $X_R$ ) in Pt-TiO<sub>2</sub> prepared at 400 °C with different doping levels.

degradation rate constants of MB,  $k_{MB}$ , under visible-light irradiation were measured as a function of the fractional content of rutile,  $X_R$ , in Pt(II)-TiO<sub>2</sub> calcined at 400 °C with different doping levels. As shown in Figure 8,  $k_{MB}$  is increased with an increasing fractional content of rutile in Pt-TiO<sub>2</sub>. This result suggests clearly that the fractional content of rutile in TiO<sub>2</sub> plays an important role in photocatalytic activity in our experiments.

TiO<sub>2</sub> particles in the rutile phase are generally considered to be much less photochemically active than their anatase phase counterparts.<sup>59–61</sup> However, there are a number of specific chemical reactions in which higher photoactivity has been reported with rutile compared to anatase.<sup>62,63</sup> For example, Kim et al.<sup>63</sup> reported that Ni-TiO<sub>2</sub> in the rutile phase had a much higher photocatalytic activity compared to the corresponding anatase phase of Ni-TiO<sub>2</sub> for the decomposition of 4-chlorophenol under both UV and visible-light irradiation. In contrast, they found the anatase phase of the undoped TiO<sub>2</sub> to have higher photocatalytic activity than undoped rutile. Furthermore, Torimoto and Ohtani<sup>59</sup> established that the photoactive crystalline phase of anatase/rutile mixed TiO<sub>2</sub> powder is clearly dependent even on the specific photocatalytic reaction (i.e., substrate or electron donor dependent). They observed that the photoreactivities of TiO<sub>2</sub> in anatase/rutile mixed phase for H<sub>2</sub> production were between pure anatase and pure rutile and shifted toward that of pure rutile with increase of rutile fraction, whereas the photoreactivities of mixed TiO<sub>2</sub> for Ag deposition and acetic acid decomposition were similar to that of pure rutile and pure anatase phases, respectively, and not dependent on the rutile fraction. In addition, it has been reported that TiO<sub>2</sub> in anatase/rutile mixed phase has higher activity than the pure anatase phase alone under UV irradiation.<sup>60,64,65</sup> Another example from our study shows that the visible-light photocatalytic activity of Pt(II)-TiO<sub>2</sub> with respect to I<sup>−</sup> oxidation is strongly influenced by the calcination temperature. The photocatalytic activity of Pt-TiO<sub>2</sub> gave a maximum at 400 °C where a mixed rutile/anatase structure of Pt-TiO<sub>2</sub> predominates. The pure anatase end member of Pt-TiO<sub>2</sub> at 200 °C and pure rutile end member of Pt-TiO<sub>2</sub> at 700 °C clearly were less photoactive than the mixed-phase structural form of Pt-TiO<sub>2</sub> at 400 °C.

Higher photocatalytic activities of Pt-TiO<sub>2</sub> or Cr-TiO<sub>2</sub> having a significant fraction of the rutile phase due to calcinations at 400 °C may be due to a larger number of oxygen vacancies.<sup>66–68</sup> For example, Li et al.<sup>68</sup> proposed that the formation of subenergy defect level in Ce-TiO<sub>2</sub> may be one of critical reasons to reduce the recombination of electron–hole pairs and to enhance

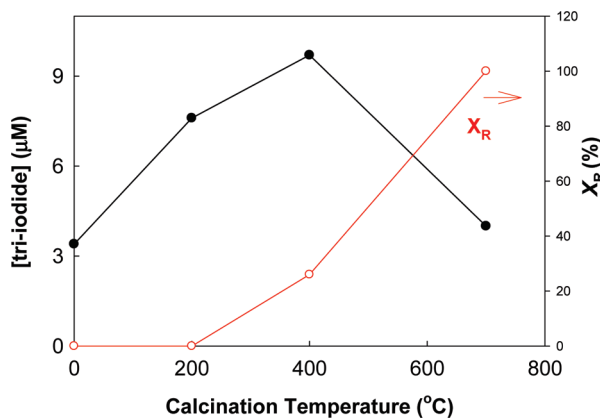


**Figure 9.** Photocatalytic activities for I<sup>−</sup> oxidation in terms of the amount of I<sub>3</sub><sup>−</sup> (μM) produced after 6 min at >400 nm irradiation and the fractions of rutile ( $X_R$ ) of 0.3 at. % Pt-TiO<sub>2</sub> as function of calcination temperature.

photocatalytic activity. Ihara et al. also reported that the oxygen-deficient TiO<sub>2</sub> induced by RF H<sub>2</sub> plasma treatment (without doping) absorbed visible light and showed visible light photocatalytic activity.<sup>69,70</sup> In a similar fashion, the formation of oxygen vacancies in Pt-TiO<sub>2</sub> or Cr-TiO<sub>2</sub>, which results in a lowering of the temperature of the A–R phase transformation leading to a rutile structure at 400 °C, appears to lead to an enhancement of the photocatalytic activities of M-TiO<sub>2</sub> under visible-light irradiation.

Our group previously investigated metal-ion doping on photocatalytic activities of TiO<sub>2</sub> under UV light irradiation in terms of the transient charge-carrier recombination dynamics.<sup>19,42,71,72</sup> Choi et al.<sup>19</sup> used laser flash photolysis measurements to show that the lifetimes of the blue electron in the Fe-, V-, Mo-, and Ru-doped TiO<sub>2</sub> were increased to ~50 ms, whereas undoped Q-sized TiO<sub>2</sub> had a shorter lifetime of <200 μs. Hoffmann and co-workers found a good correlation between experimental quantum yields for oxidation or reduction and the measured absorption signals of the charge carriers that survived from recombination over the nano- to microsecond time domain (i.e., an increase in concentration of the long-lived charge carriers is expected to result in higher photoreactivity). In addition, Martin et al.<sup>42,71,72</sup> used time-resolved microwave conductivity (TRMC) measurements of various TiO<sub>2</sub> samples including V-TiO<sub>2</sub> and Fe-TiO<sub>2</sub>. The charge-carrier recombination lifetime and the interfacial electron-transfer rate constants were estimated from the decays of TRMC signals and also found to correlate well with measured quantum efficiencies. Furthermore, in the case of V-doped TiO<sub>2</sub>, photoreactivity also appeared to be a function of sintering temperatures.<sup>42</sup> For examples, V(IV) is found to reduce the photoreactivity of TiO<sub>2</sub> by promoting charge-carrier recombination via electron trapping at >VO<sub>2</sub><sup>+</sup> present in V-TiO<sub>2</sub> (25 °C) or via hole trapping at V(IV) impurities in surficial V<sub>2</sub>O<sub>5</sub> islands on V-TiO<sub>2</sub> (200 or 400 °C), whereas in the case of V-TiO<sub>2</sub> prepared at 600 or 800 °C, substitutional V(IV) in the lattice of TiO<sub>2</sub> appears to act as a charge-carrier recombination center that resulted in reduced photoreactivity. The above observations emphasize that metal-ion dopants influence the photoreactivity of TiO<sub>2</sub> by altering the charge-carrier recombination and interfacial charge-transfer rate constants. In conclusion, we believe that these effects are also important for the M-TiO<sub>2</sub> materials prepared as part of this study as well.

## Conclusions

In conclusion, we have synthesized an array of metal-doped titanium dioxide materials, M-TiO<sub>2</sub>, in order to evaluate their

visible-light photocatalytic activities. Pt-, Cr-, V-, Fe-, Rb-, Y-TiO<sub>2</sub> lowered the temperature of the anatase-to-rutile phase transformation, whereas Ru-TiO<sub>2</sub> increased the temperature of the A-R phase transformation. The fraction of rutile in M-TiO<sub>2</sub> is observed to be dependent on the doping level. However, there appears to be no correlation between the effectiveness of an individual dopant on the A-R phase transformation and its valence state or ionic radius as previously suggested.<sup>47,48</sup> The majority of M-TiO<sub>2</sub> materials prepared herein gave absorption spectra that were extended into the visible region beyond 400 nm. Ag-, Rb-, Y-, and La-TiO<sub>2</sub> did not change the original absorption spectrum of pristine SG-TiO<sub>2</sub>. As verified by EDS analysis, the latter group of ions were most likely not incorporated into the lattice of TiO<sub>2</sub> and were most likely concentrated in the near surface region because of their relatively large ionic radii. The photocatalytic activities of M-TiO<sub>2</sub> were evaluated for MB degradation, I<sup>-</sup> oxidation, and phenol degradation under visible-light irradiation at  $\lambda > 400$  nm. Pt-TiO<sub>2</sub> and Cr-TiO<sub>2</sub>, which were prepared at a 0.3 at. % doping level and annealed at 400 °C, had a relatively high fraction of rutile and showed significantly enhanced photocatalytic activity compared to SG-TiO<sub>2</sub> for all test reactions under visible-light irradiation. These results indicate that the presence of the rutile structure in the doped TiO<sub>2</sub> may affect photocatalytic activities of M-TiO<sub>2</sub>. Pt-TiO<sub>2</sub> substantially improved the observed photocatalytic activity under UV irradiation at  $\lambda > 320$  nm as well. On the other hand, V-, Rb-, Ni-, and Fe-TiO<sub>2</sub> showed visible-light photocatalytic activities only for one or two of the three test reactions.

**Acknowledgment.** We gratefully acknowledge the generous support for this research that has been provided by the Northrop-Grumman Corporation. In particular, we give special credit to Dr. Ronald Pirich for his enthusiastic encouragement and intellectual support for our joint projects over the years.

**Supporting Information Available:** Energy dispersive spectra for Pt(II)-TiO<sub>2</sub> and La-TiO<sub>2</sub>. This material is available free of charge via the Internet at <http://pubs.acs.org.org>.

## References and Notes

- Zhang, X. W.; Lei, L. C. *Mater. Lett.* **2008**, *62*, 895.
- Nahar, S.; Hasegawa, K.; Kagaya, S. *Chemosphere* **2006**, *65*, 1976.
- Zhu, J. F.; Chen, F.; Zhang, J. L.; Chen, H. J.; Anpo, M. *J. Photochem. Photobiol., A* **2006**, *180*, 196.
- Niiшиro, R.; Kato, H.; Kudo, A. *Phys. Chem. Chem. Phys.* **2005**, *7*, 2241.
- Kim, D. H.; Lee, K. S.; Kim, Y. S.; Chung, Y. C.; Kim, S. J. *J. Am. Ceram. Soc.* **2006**, *89*, 515.
- Iketani, K.; Sun, R. D.; Toki, M.; Hirota, K.; Yamaguchi, O. *Mater. Sci., B* **2004**, *108*, 187.
- Klosek, S.; Raftery, D. *J. Phys. Chem. B* **2001**, *105*, 2815.
- Wu, J. C. S.; Chen, C. H. *J. Photochem. Photobiol., A* **2004**, *163*, 509.
- Borgarello, E.; Kiwi, J.; Gratzel, M.; Pelizzetti, E.; Visca, M. *J. Am. Chem. Soc.* **1982**, *104*, 2996.
- Anpo, M.; Ichihashi, Y.; Takeuchi, M.; Yamashita, H. *Sci. Technol. Catal.* **1999**, *121*, 305.
- Pan, C. C.; Wu, J. C. S. *Mater. Chem. Phys.* **2006**, *100*, 102.
- Asahi, R.; Morikawa, T.; Ohwaki, T.; Aoki, K.; Taga, Y. *Science* **2001**, *293*, 269.
- Gole, J. L.; Stout, J. D.; Burda, C.; Lou, Y. B.; Chen, X. B. *J. Phys. Chem. B* **2004**, *108*, 1230.
- Mrowetz, M.; Balcerki, W.; Colussi, A. J.; Hoffman, M. R. *J. Phys. Chem. B* **2004**, *108*, 17269.
- Umebayashi, T.; Yamaki, T.; Tanaka, S.; Asai, K. *Chem. Lett.* **2003**, *32*, 330.
- Wang, Y.; Meng, Y. L.; Ding, H. M.; Shan, Y. K.; Zhao, X.; Tang, X. Z. *J. Phys. Chem. C* **2008**, *112*, 6620.
- Yang, X.; Cao, C.; Hohn, K.; Erickson, L.; Maghirang, R.; Hamal, D.; Klabunde, K. J. *Catal.* **2007**, *252*, 296.
- Tachikawa, T.; Tojo, S.; Kawai, K.; Endo, M.; Fujitsuka, M.; Ohno, T.; Nishijima, K.; Miyamoto, Z.; Majima, T. *J. Phys. Chem. B* **2004**, *108*, 19299.
- Choi, W.; Termin, A.; Hoffmann, M. R. *J. Phys. Chem.* **1994**, *98*, 13669.
- Karakitsou, K. E.; Verykios, X. E. *J. Phys. Chem.* **1993**, *97*, 1184.
- Soria, J.; Conesa, J. C.; Augugliaro, V.; Palmisano, L.; Schiavello, M.; Sclafani, A. *J. Phys. Chem.* **1991**, *95*, 274.
- Chen, J. H.; Yao, M. S.; Wang, X. L. *J. Nano. Res.* **2008**, *10*, 163.
- Di Paola, A.; Garcia-Lopez, E.; Ikeda, S.; Marci, G.; Ohtani, B.; Palmisano, L. *Catal. Today* **2002**, *75*, 87.
- Kim, S.; Hwang, S. J.; Choi, W. *J. Phys. Chem. B* **2005**, *109*, 24260.
- Ohno, T.; Tanigawa, F.; Fujihara, K.; Izumi, S.; Matsumura, M. *J. Photochem. Photobiol., A* **1999**, *127*, 107.
- Amadelli, R.; Samiolo, L.; Maldotti, A.; Molinari, A.; Valigi, M.; Gazzoli, D. *Int. J. Photoenergy* **2008**, *853753*.
- Iwasaki, M.; Hara, M.; Kawada, H.; Tada, H.; Ito, S. *J. Colloid Interface Sci.* **2000**, *224*, 202.
- Anpo, M. *Pure Appl. Chem.* **2000**, *72*, 1787.
- Amadelli, R.; Samiolo, L.; Maldotti, A.; Molinari, A.; Valigi, M.; Gazzoli, D. *Int. J. Photoenergy* **2008**, *9*.
- Lettmann, C.; Hinrichs, H.; Maier, W. F. *Angew. Chem., Int. Ed.* **2001**, *40*, 3160.
- Woodhouse, M.; Parkinson, B. A. *Chem. Soc. Rev.* **2009**, *38*, 197.
- Sohn, J. M.; Oh, K. S.; Woo, S. I. *Korean J. Chem. Eng.* **2004**, *21*, 123.
- Ding, Z.; Lu, G. Q.; Greenfield, P. F. *J. Phys. Chem. B* **2000**, *104*, 4815.
- Jing, L. Q.; Sun, X. J.; Xin, B. F.; Wang, B. Q.; Cai, W. M.; Fu, H. G. *J. Solid State Chem.* **2004**, *177*, 3375.
- Pillai, S. C.; Periyat, P.; George, R.; McCormack, D. E.; Seery, M. K.; Hayden, H.; Colreavy, J.; Corr, D.; Hinder, S. J. *J. Phys. Chem. C* **2007**, *111*, 1605.
- Anderson, C.; Bard, A. J. *J. Phys. Chem. B* **1997**, *101*, 2611.
- Spurr, R. A.; Myers, H. *Anal. Chem.* **1957**, *29*, 760.
- Ghosh, S. K.; Vasudevan, A. K.; Rao, P. P.; Warrier, K. G. K. *Br. Ceram. Trans.* **2001**, *100*, 151.
- Borkar, S. A.; Dharwadkar, S. R. *J. Therm. Anal. Calorim.* **2004**, *78*, 761.
- Matteucci, F.; Cruciani, G.; Dondi, M.; Raimondo, M. *Ceram. Int.* **2006**, *32*, 385.
- Iida, Y.; Ozaki, S. *J. Am. Ceram. Soc.* **1961**, *44*, 120.
- Martin, S. T.; Morrison, C. L.; Hoffmann, M. R. *J. Phys. Chem.* **1994**, *98*, 13695.
- Ruiz, A. M.; Sakai, G.; Cornet, A.; Shimano, K.; Morante, J. R.; Yamazoe, N. *Sens. Actuators, B* **2003**, *93*, 509.
- Sibu, C. P.; Kumar, S. R.; Mukundan, P.; Warrier, K. G. K. *Chem. Mater.* **2002**, *14*, 2876.
- Ruiz, A. M.; Cornet, A.; Morante, J. R. *Sens. Actuators, B* **2004**, *100*, 256.
- Ogata, S.; Iyetomi, H.; Tsuruta, K.; Shimojo, F.; Nakano, A.; Kalia, R. K.; Vashishta, P. *J. Appl. Phys.* **2000**, *88*, 6011.
- Shannon, R. D.; Pask, J. A. *J. Am. Ceram. Soc.* **1965**, *48*, 391.
- Mackenzie, K. J. D. *Trans. J. Br. Ceram. Soc.* **1975**, *74*, 29.
- Umebayashi, T.; Yamaki, T.; Itoh, H.; Asai, K. *J. Phys. Chem. Solids* **2002**, *63*, 1909.
- Zhao, Z. Y.; Liu, Q. J.; Zhang, J.; Zhu, Z. Q. *Acta Phys. Sin.* **2007**, *56*, 6592.
- Kudo, A.; Niiшиro, R.; Iwase, A.; Kato, H. *Chem. Phys.* **2007**, *339*, 104.
- Kuznetsov, V. N.; Serpone, N. *J. Phys. Chem. B* **2006**, *110*, 25203.
- Serpone, N. *J. Phys. Chem. B* **2006**, *110*, 24287.
- Lisachenko, A. A.; Kuznetsov, V. N.; Zakharov, M. N.; Mikhailov, R. V. *Kinet. Catal.* **2004**, *45*, 189.
- Kuznetsov, V. N.; Krutitskaya, T. K. *Kinet. Catal.* **1996**, *37*, 446.
- Yan, X. L.; Ohno, T.; Nishijima, K.; Abe, R.; Ohtani, B. *Chem. Phys. Lett.* **2006**, *429*, 606.
- Ohno, T.; Tsubota, T.; Nishijima, K.; Miyamoto, Z. *Chem. Lett.* **2004**, *33*, 750.
- Bettinelli, M.; Dallacasa, V.; Falcomer, D.; Fornasiero, P.; Gombac, V.; Montini, T.; Romano, L.; Speghini, A. *J. Hazard. Mater.* **2007**, *146*, 529.
- Torimoto, T.; Nakamura, N.; Ikeda, S.; Ohtani, B. *Phys. Chem. Chem. Phys.* **2002**, *4*, 5910.
- Zhang, Q. H.; Gao, L.; Guo, J. K. *Appl. Catal., B* **2000**, *26*, 207.
- Lucarelli, L.; Nadtochenko, V.; Kiwi, J. *Langmuir* **2000**, *16*, 1102.
- Addamo, M.; Bellardita, M.; Di Paola, A.; Palmisano, L. *Chem. Commun.* **2006**, 4943.
- Kim, D. H.; Choi, D. K.; Kim, S. J.; Lee, K. S. *Catal. Commun.* **2008**, *9*, 654.

- (64) Bakardjieva, S.; Subrt, J.; Stengl, V.; Dianez, M. J.; Sayagues, M. J. *Appl. Catal., B* **2005**, *58*, 193.
- (65) Jung, K. Y.; Park, S. B. *J. Photochem. Photobiol., A* **1999**, *127*, 117.
- (66) Yang, J.; Bai, H. Z.; Jiang, Q.; Lian, H. S. *Thin Solid Films* **2008**, *516*, 1736.
- (67) Kim, H. Y.; Lee, H. M.; Pala, R. G. S.; Shapovalov, V.; Metiu, H. *J. Phys. Chem. C* **2008**, *112*, 12398.
- (68) Li, F. B.; Li, X. Z.; Hou, M. F.; Cheah, K. W.; Choy, W. C. H. *Appl. Catal., A* **2005**, *285*, 181.
- (69) Ihara, T.; Miyoshi, M.; Ando, M.; Sugihara, S.; Iriyama, Y. *J. Mater. Sci.* **2001**, *36*, 4201.
- (70) Ihara, T.; Miyoshi, M.; Iriyama, Y.; Matsumoto, O.; Sugihara, S. *Appl. Catal., B* **2003**, *42*, 403.
- (71) Martin, S. T.; Herrmann, H.; Choi, W. Y.; Hoffmann, M. R. *J. Chem. Soc., Faraday Trans.* **1994**, *90*, 3315.
- (72) Martin, S. T.; Herrmann, H.; Hoffmann, M. R. *J. Chem. Soc., Faraday Trans.* **1994**, *90*, 3323.

JP908088X